

Explication of Extrinsic Forearm Muscles On the Classification of Thumb Position Using High-Density Surface Electromyogram

M.M Suhaimi¹, A.S. Ghazali^{1*}, A. Jazlan¹, S.N. Sidek¹

¹International Islamic University Malaysia, Kuala Lumpur, MALAYSIA

*Corresponding Author

DOI: <https://doi.org/10.30880/ijie.2023.15.01.002>

Received 19 May 2021; Accepted 25 May 2021; Available online 28 February 2023

Abstract: Muscles for hand functions and movements play a major role in basic daily activities such as writing and lifting objects. The main digit of the finger in differentiating the hand gesture is the thumb and its main muscles are intrinsic muscles. However, for transradial amputees, despite the loss of access to the intrinsic muscles, any information from the extrinsic muscles would be paramount and non-negotiable in creating a perfect hand prosthesis. As such, the research is dedicated to study the relationship between extrinsic muscles located at human's forearm to characterize the actual thumb attitudes. A 64-channel HD-sEMG recording device together with a thumb force measuring platform was utilized to collect the required signals from 17 participants at several thumb angle positions namely zero-degrees, thirty-degree, sixty-degrees, and ninety-degree. For each position, the participants were required to place their thumbs on top of a load cell at relax (no force at all) and contact (30% of their individual Maximum Voluntary Contraction or known as MVC) conditions repetitively by following a designated trajectory. Feature extraction was performed by calculating the Root Mean Square (RMS) values of the HD-sEMG data collected from each channel. Six different classifiers have been used to classify the relationship between the forearm HD-sEMG and the corresponding thumb positions. As a result, LazyIBK obtained the highest correctly classified instances with 81.05%. The finding is significant in developing a dedicated control framework for a prosthetic hand for transradial amputees that can operate as closely as normal.

Keywords: Thumb position, HD-sEMG, extrinsic, upper-limb myoelectric prosthetic

1. Introduction

Contributions of the thumb towards hand functions and movements are inherently indispensable especially since the thumb is the only opposable digit that plays a crucial role in all facets of grip formation. Injury or loss of function of the thumb can severely limit overall hand function and movements [1]. A study by Park et al [2] reported that thumb corresponds to at least 50% of hand functions. The groups of muscles that control the movements of fingers and overall hand grip strength can be divided into two categories namely extrinsic and intrinsic muscles. These muscles play a vital role in exerting the strength of the opposing grip and also the position of the thumb. The synergistic combination between extrinsic and intrinsic muscles enables control of the digits, thumb, and the amount of force that can be exerted by both the digits and the thumb.

A study conducted by Ziegler-Graham et al. [3] estimated the prevalence of limb loss in the United States in 2005 is 1.6 million peoples. Importantly, the numbers were projected to be doubled by 2050. The common loss of limbs is due to accidents, wars, and diseases. There are also cases where a person is born without a perfect hand. There are two common amputations for them namely transradial and transcarpal, as demonstrated in figures 1. Transradial amputation happens at the forearm area and the cuts are generally made in a ratio of 1 to 1 of the forearm length and interconnection

between intrinsic and extrinsic sets of muscles is lost. Transcarpal amputation is a common type of amputation and occurs for a variety of reasons such as diabetes and also an accident that will eventually force amputation in some patients. After all, transcarpal amputation is found to be better than transradial amputation because flexion and extension of the wrist are still preserved and overall hand function can be preserved [4].

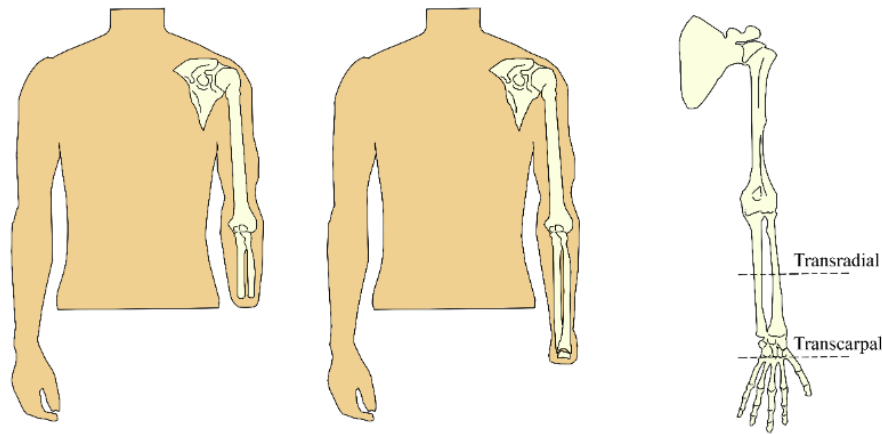


Fig 1 - Transcarpal and transradial amputations

There is a continuous development of cybernetic hands to create a perfect function of hand prosthesis to be used for people in transradial and transcarpal amputation conditions. The current prosthesis hand in the market is limited only to grasp activities due to the limitations of information obtained from the arm in identifying the thumb attitudes [5]. The development of ‘perfect’ cybernetic hands are hindered due to the small size of flexor pollicis longus which is the muscles that contribute to controlling thumb attitude, also the location of the muscle very deep from the skin’s surface, and each muscle is close with one another especially with flexor digitorum profundus located next to it and also flexor digitorum superficialis located above it [6]. These issues lead to difficulties in identifying the stimulation of individual muscles.

Muscle activity of the forearm can be measured and analysed using surface Electromyogram (sEMG) signals. sEMG signals are extracted due to electrical manifestations of contracted muscle-related neuromuscular stimulation [7]. These signals are produced by the electrical activity of the accumulation of motoneuron-excited muscle fibers. Previous studies demonstrated the feasibility of sEMG signals for the control of robotic hand prostheses [8,9,10]. They are 4 muscles that contribute to thumb attitude at the forearm area namely Flexor Pollicis Longus (FPL), Abductor Pollicis Longus (APL), Extensor Pollicis Longus (EPL), and Extensor Pollicis Brevis (EPB) as illustrated in figures 2. However, the Flexor Pollicis Longus (FPL) has been extensively used for the control of robotic hand prostheses [11, 12].

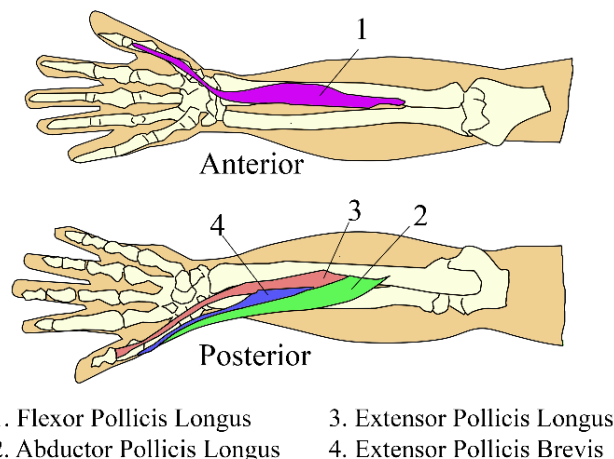


Fig. 2 - Thumb extrinsic muscles

Continuous research and development have revealed limitations in the analysis of sEMG such as information only from the placement of the electrode and it does not indicate the whole activity of the muscles [13]. These limitations have led to a better-developed technology known as High-Density surface Electromyogram (HD-sEMG) [14]. HD-sEMG has many similarities to ordinary sEMG measurements, the main difference being that smaller electrodes are densely arranged in a grid positioned along the region of interest enabling more information to be obtained from that region of muscles

under investigation. A study conducted by Cavalcanti Garcia and Vieira [13] highlighted some advantages of using HD-sEMG compared to normal surface EMG. The first advantage is based on myoelectric activity detected atomical and further physiological indications that can be obtained when multiple electrodes are used at the location of tendons and end-plates, as well as the length of muscle fibres. Also, by using HD-sEMG, the actual position of the muscles can be detected more accurately than sEMG. Thus, the problem of placement mismatch for a single sEMG can be overcome. Other than that, in case an array of surface electrodes was placed on the skin parallel to the path of the muscle fibres, each electrode will report a delayed version of the Motor Unit Action Potentials (MUAPs). So, the conduction velocity of action potentials propagating along the muscle fibres can only be measured afterward. Interestingly, the delay can be minimized or omitted using HD-sEMG technology.

For transradial and transcarpal amputees, the HD-sEMG recordings can be obtained from the amputee's stump, residual limbs, or other muscles that were not affected by the amputation activity. With the development of efficient machine learning algorithms that capable to handle large datasets, HD-sEMG has a bright potential to complement or eventually replace sEMG as control signals for robotic prostheses [15]. To extract important information from raw data, there is a step called feature extraction, and the most significant features will be used to feed the classifier in forming classes for the dataset [14,15]. Features can be extracted using time, frequency, and time-frequency domains. Due to its mathematical simplicity and good performance, time-domain (TD) features are commonly used [18]. TD features are determined based on the amplitude of the signals and do not require any complicated measurement and frequently used TD feature is Root Mean Square (RMS) [2,17] and mean absolute value [15,18], while frequency-domain (FD) characteristics are based on the frequency range and calculated based on the Fourier transformation and frequently features used are mean frequency [16,19] and median frequency [16,20]. The results of the study conducted by Siddiqi and Sidek [17] showed TD analysis produces higher accuracy to differentiate different finger attitudes than FD.

Classification is a valuable technique to describe the action of complex nonlinear processes in the presence of conventional mathematical models [23], and it is also a promising technique to be used as part of a cybernetic prosthesis control algorithm. Classification algorithms consist of three types, namely supervised, unsupervised learning, and reinforcement learning [22,23]. Previous studies have used various classifiers such as Neural Network (NN), Support Vector Machine (SVM), and Linear Discriminant Analysis (LDA). As the result, all the classifiers performance show accuracy above 89%, however, there is not a single best classifier as it depends on the data set [2,26]. The results of different classification algorithms are compared to find which algorithm produces effective results. In particular, there are three forms of classification for the collected HD-sEMG data namely HD-EMG map intensity classification, HD-EMG map intensity and center of gravity classification, and single differential channel intensity classification. The last form was recommended as the best standard classification technique [16].

In this paper, an experimental setup was developed to simultaneously measure and analyze forearm HD-sEMG signals for the anterior compartment. For the experimental procedure, the force exerted by the thumb was fixed to 30% Maximum Voluntary Contraction (MVC) as recommended by Aranceta-Garza [2]. There are four thumb positions under study which are zero-degrees, thirty-degree, sixty-degrees, and ninety-degree. Feature extraction was then performed on the collected data by using the RMS values of the HD-sEMG readings from each channel. After that, the machine learning classification was performed using the Weka open-source machine learning software. By using several machine learning algorithms such as ZeroR, Reduced Error Pruning Tree (REPTree), Multi-Class Classifier, Filtered Classifier, Random Forest, and LazyIBK (K-nearest Neighbour), the HD-sEMG data was classified according to the respective thumb positions.

2. Methods

2.1 Research Subjects / Participants

This experimental work was approved by the International Islamic University of Malaysia Research Ethics Committee (Approval ID: 2020-080). A total of 17 participants were involved (14 males, 3 females; age 26.5 ± 3.5 years). Before the experiment started, all participants required to read and grant their written consent besides declared that they have no prior history of nerve injury, hand surgery, and/or accidents. The participants were randomly selected among International Islamic University Malaysia students. The duration of the experiment conducted on each subject lasted for an hour.

2.2 HD-sEMG Recording Setup and Electrode Placement

A portable biomedical signal amplifier (Model Name: Sessantaquattro) manufactured by OT-Bioelettronica was used to capture 64 channels of monopolar HD-sEMG signals. An HD-sEMG electrode pad consists of 13 rows and 5 columns grids with an 8 mm inter-electrode distance was placed on the anterior side of the participant's forearm (Part Number: GR08MM1305). As described by Bao et al [27], the most appropriate electrode placement on the forearm for both finger extension and flexion for the x-axis is located between the coordinate -2 and 0 for the anterior compartment while for the y-axis, the best placement of electrodes is between the coordinate of 4 to 12 as illustrated in Fig 3. In line with the suggested placement, a uniform electrode pad was located between the ulnar head and the elbow crease of the participant's

forearm mapped the location of the anterior musculature. As shown in Fig 4, the corresponding pad was aligned 25% from the proximal landmark to a virtual line.

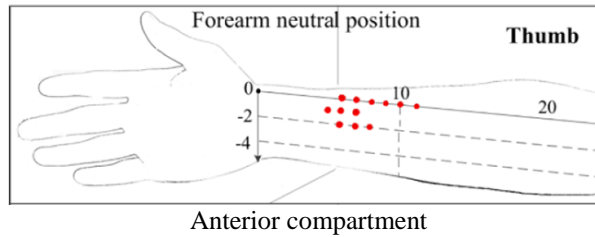


Fig 3 - Grid electrode placement on the anterior musculature. This image is taken from Bao et al [27].

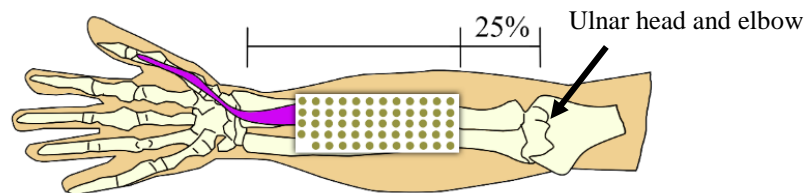


Fig 4 - Electrode placement: illustration of 25% from ulnar head and elbow

The placement of the pad was standardized for each subject; depending on the dimensions of his or her arm length and circumference. The pad was firmly secured on top of the participant's skin using a Velcro strap to minimize the effects of motion artifacts. Following a standard sEMG measurement procedure, skin preparation was firstly carried out by using an alcohol-based solution [28],[29].

2.3 Thumb Force Measuring Platform

The thumb force measuring platform was developed with a load cell to measure the applied force, an op amp-based signal conditioning circuit to filter unwanted signals, and an Arduino microcontroller to display the readings from the load cell through the computer (with Matlab software installed). Importantly, the developed platform can be adjusted such that the position of the thumb is fixed at zero-degrees, thirty-degree, sixty-degrees, and ninety-degree as shown in Fig 5. The platform used in this study called adjustable portable thumb muscles system as demonstrated in Fig 6.

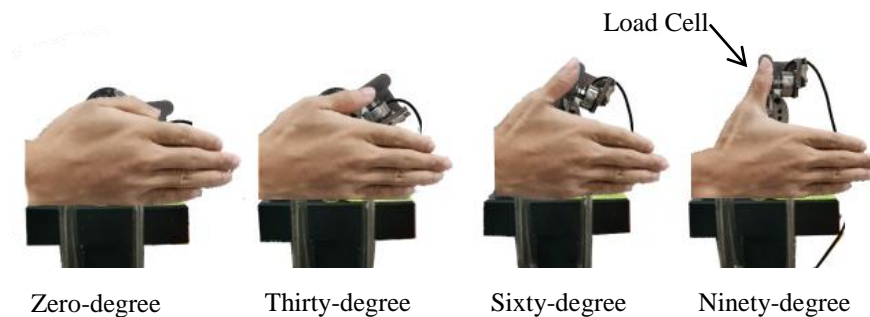


Fig 5 - Various positions of the thumb exertion on the load cell

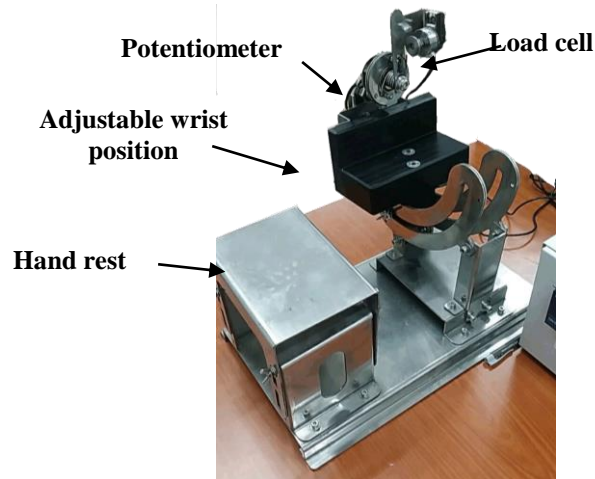


Fig 6 - Portable thumb muscles system

2.4 Experimental Setup

First, the participant was asked to fill up a consent form which was approved by IIUM Research Ethics Committee. After that, the experimenter measured the forearm length of the participant for electrode placement intent before placing an HD-sEMG electrodes pad at the anterior side of the participant's hand following the 25% rules shown in Fig 4. Next, the participant was asked to sit in front of a dedicated computer display before the experimenter adjusted the position of the participant's upper arm, forearm, and wrist to be placed appropriately on a constructed adjustable portable thumb muscles system as demonstrated in Fig 6. The experiment was conducted using the right arm of the participants, which was placed at 90° shoulder abduction, 90° elbow flexion, and neutral location of the wrist as shown in Fig 7. The experiment started once the Maximum Voluntary Contraction (MVC) of individual participants measured by the load cell.

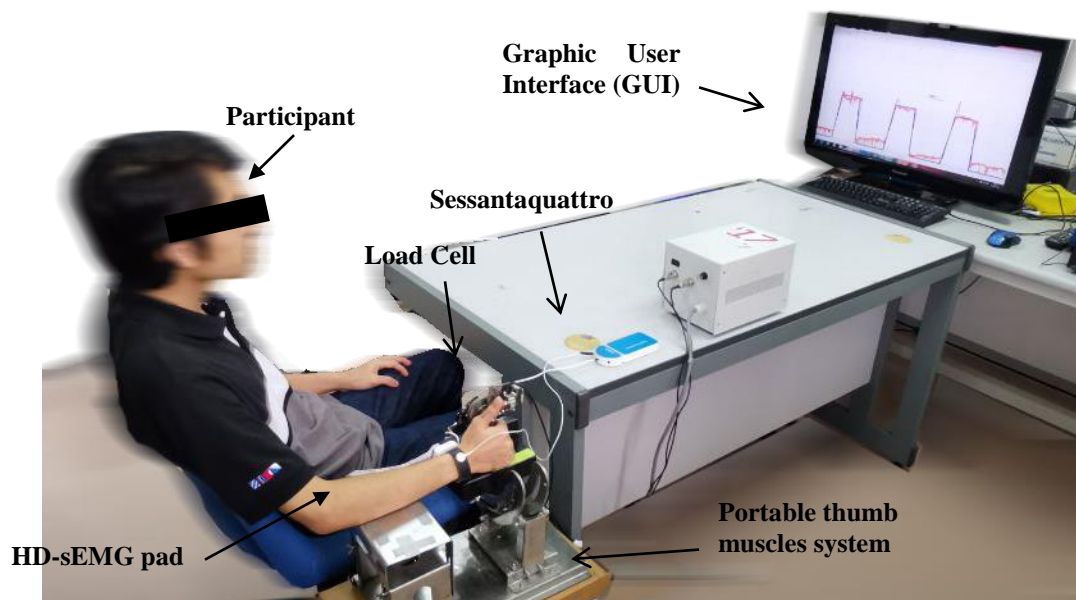


Fig 7 - Experiment setup to collect the HD-sEMG signals recording

For a specific thumb angle position (e.g. zero-degree), the participant was asked to place the thumb without any force for eight seconds (rest condition) before exerted 30% MVC of thumb force (contract condition) for five seconds. A Matlab program has been written to calculate 30% of the MVC at each of these thumb positions for each subject respectively. As shown in Graphical User Interface (GUI) in Fig 8, the participant was required to apply the force by following the trajectory: rest-contract-rest-contract-rest-contract-rest for a complete cycle of the experiment. The force exerted by the thumb at the specific angle positions was measured by the same load cell as the MVC measurement, and the output of the hand force was displayed in real-time. From Fig 8, it can be seen that the actual thumb force measured by the load cell has fluctuations both during 30% MVC muscle activity and also during rest intervals.

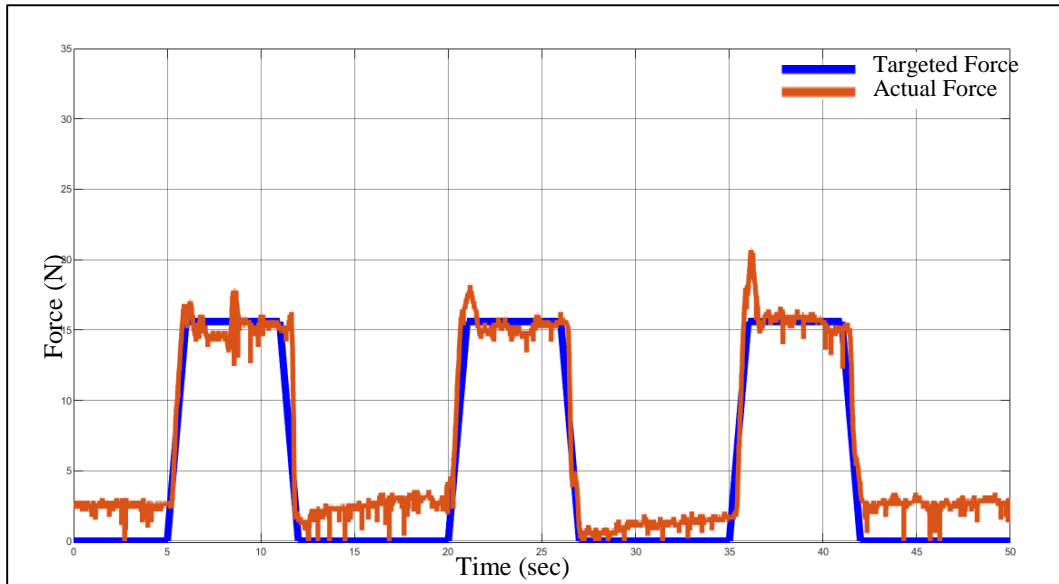


Fig 8 - The trajectory of the rest and contract conditions

For repeatability purposes, readings for each thumb angle position were repeated three times. That is, in a zero-degree thumb angle position, three complete cycles (three records) of the experiment were conducted. Overall, the same procedures were repeated for other thumb angle positions (thirty-degree, sixty-degree, and ninety-degree). The flowchart for the data collection process is illustrated in Fig 9.

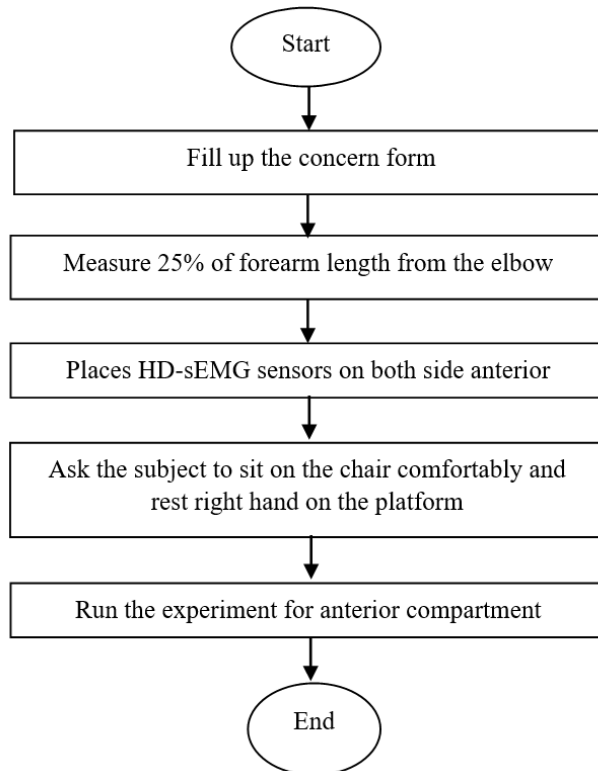


Fig 9 - Data collection procedure

Table 1 shows the amount of exerted force (at various thumb angle positions) corresponding to 30% of the MVC readings obtained from 17 participants.

Table 1 - Description of the participants with 30% MVC values for each thumb angle position

Participant ID	Gender	Age	30% MVC (N)			
			Zero-degree	Thirty-degree	Sixty-degree	Ninety-degree
1	Male	26	11.84	11.49	10.57	18.1
2	Male	26	8.56	9.538	12.35	19.31
3	Male	30	8.15	10.24	14.48	18.44
4	Male	27	7.97	12.28	12.17	14.87
5	Male	25	7.68	11.02	14.7	16.99
6	Male	24	8.26	9.24	10.9	13.78
7	Male	25	7.89	11.23	12.5	17.56
8	Male	26	6.98	8.21	10.35	11.68
9	Male	26	7.84	7.98	9.84	10.96
10	Male	25	8.45	9.42	12.82	12.35
11	Male	28	7.87	7.98	9.93	10.67
12	Male	27	7.46	8.38	11.87	12.91
13	Female	25	7.05	6.71	6.01	16.02
14	Female	30	2.39	5.1	5.559	6.996
15	Female	25	6.42	6.43	6.938	8.547
16	Female	27	5.48	5.89	6.53	7.03
17	Female	26	6.67	6.86	7.54	7.81

3. Result and Discussion

3.1 Amplitude Signal Analysis and Feature Extraction

64 channels HD-sEMG signals were acquired at a sampling frequency of 2,000 samples per second. Based on the sampled readings, iso-potential maps computed from the average RMS values from each channel of the HD-sEMG were constructed. Fig 10 shows the example of iso-potential maps generated from the variation of the magnitude localized at zero-degree, thirty-degree, sixty-degree, and ninety-degree angles resulting from 30% MVC. As result, 9,792 vectors (64 electrodes \times 153 repetitions) were extracted from a single angle.

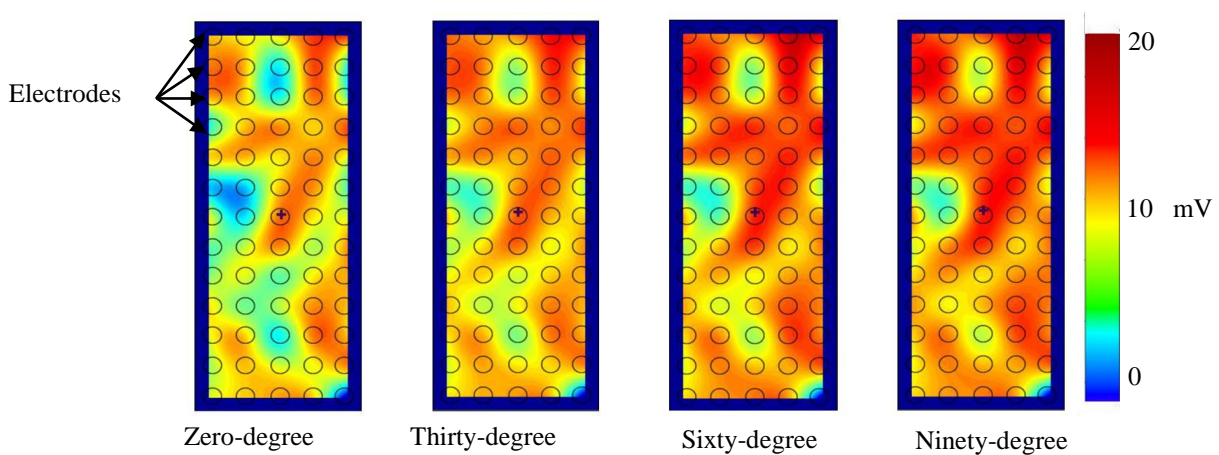


Fig 10 - Iso-potential maps generated from average RMS values based on the amplitude of the HD-sEMG signals from each electrode (mV). Multiple circles in the picture indicate EMG electrodes.

3.2 Feature Extraction

RMS sEMG amplitude analysis is also known as envelope signal analysis. For this study, instead of averaging the data, RMS was selected as a feature due to its non-zero values [30]. Also, the RMS values were found to be significantly important to distinguish the state of the muscles: either in contract or relax condition. As illustrated in Fig 11, RMS values for the contract condition showed higher amplitudes than the relax condition due to high ion flows in between the muscle fibres in the contract condition.

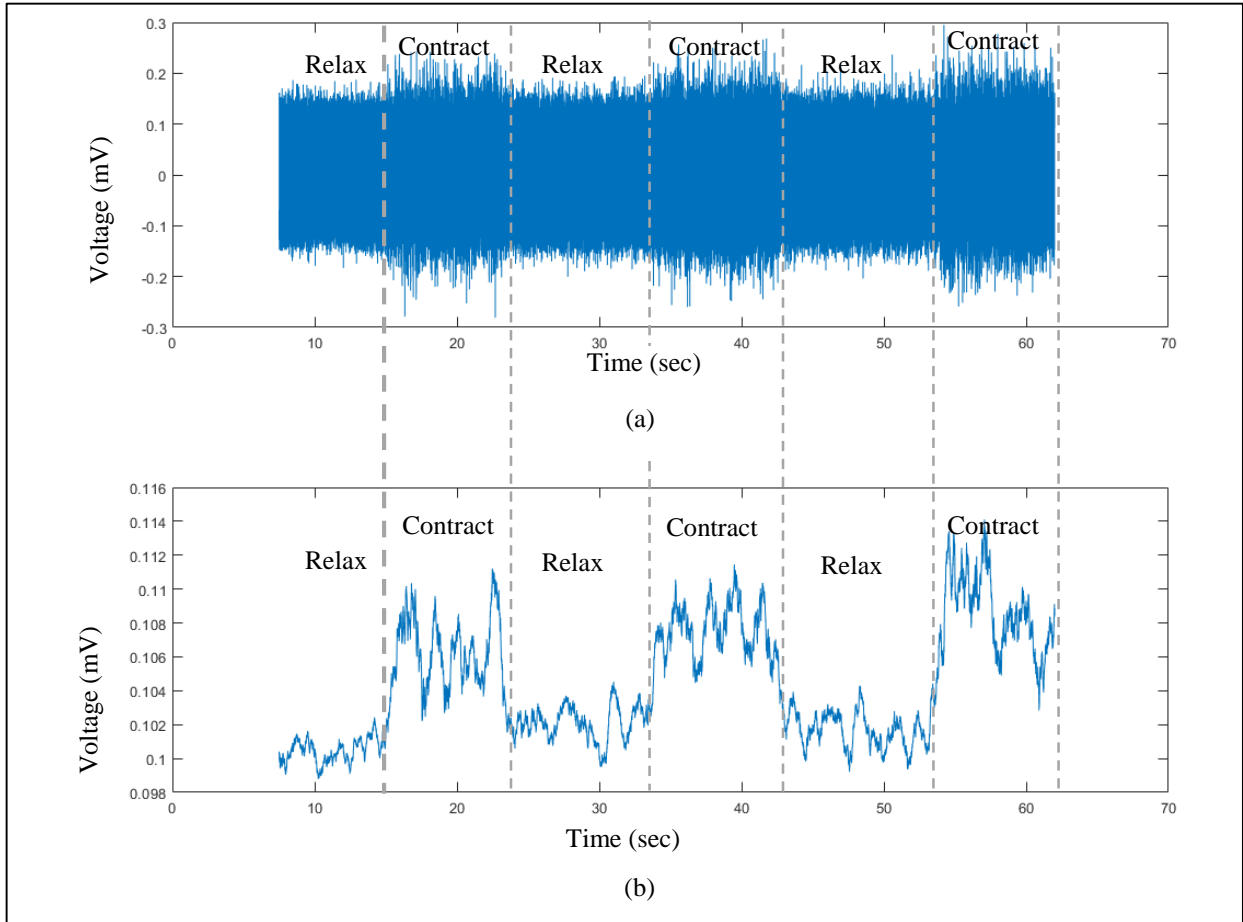


Fig 11 - EMG signal for a single electrode (a) RAW signal; (b) enveloped signal that differentiates contract and relaxes conditions

Inconsistent data can trigger several issues during the classification process, so logical and reliable data is important in a relational database. A poor, inconsistent EMG database may provide incorrect details, and to a certain extent, fail to be analysed properly [31]. As such, the RMS values were normalized in the next pre-processing step to introduce consistency since each participant has unique RMS values due to individual 30% MVC resulting in distinctive isometric maps. The normalization approach can minimize the effects of muscle shift under the skin and amplitudes on regional EMG activity [32]. In this step, the average normalized RMS values (indicated as \bar{x}) of individual 64 channels (indicated as n : data from n^{th} electrode out of 64 electrodes) for each dataset (each participant) were calculated in percentage form using Formula 1 Eq. (1).

$$\frac{n}{\bar{x}} \times 100\% \quad (1)$$

After that, the normalized RMS values were grouped into several numerical values to avoid the usage of redundant features [20]. In this step, the data were grouped into the increment grouping of 1 (non-grouping), 2, 3, and 4; with the initial value for each group started with 10 and end with ± 160 . For example, in grouping 4, the data was set to start with 10 and the next number will be 14,18 up to 162. So, in case the data is in the range of 11 to 14, the data will be set to 14 reflecting the highest number of the specific range. Whereas in case the data is in the range of 15 to18, then the data will

be set to 18. The best increment group number was selected depending on the accuracy acquired after the data was fed to the classifier. However, for test purposes, grouping 4 was selected as the increment group in the data analysis.

3.3 Classification

In the absence of standard mathematical models, classification is an essential method in identifying and understanding the behaviour of dynamic nonlinear processes [33]. The pre-processed data (or instances) in this study were analyzed using an open-source machine learning tool known as Weka 3 software [34]. By default, the test option of the software set as cross-validation folds 10. This setting was divided the data set into ten pieces then one of the data was set as testing and nine for training. After the first training and testing process, the testing pieces changed to the other pieces and other nine become training set and overall the process take 10 time until all the pieces has become part of the testing. The end of the process each pieces of data set has used once as testing set and 9 for training set. The result will be average of all 10 tests [35].

Table 2 summarizes the percentage classifications obtained from using an increment of group 4 for several types of classifiers namely Lazy.IBK, Random Forest, Filtered Classifier, Multi-Class Classifier, REP Tree, and ZeroR classifiers.

Table 2 - Percentage correctly (and incorrectly) classified instances for tested classifiers

	Type of classifier	Correctly Classified Instances (%)	Incorrectly Classified Instances (%)
1	Lazy IBK	74.65	25.35
2	Random Forest	72.80	27.2
3	Filtered Classifier	47.45	52.55
4	Multi Class Classifier	53.47	46.53
5	REP Tree	55.79	44.21
6	ZeroR	11.57	88.43

As result, Lazy.IBK scored the highest correctly classified instances among other classifiers (74.65%) followed by Random Forest (72.80%). Results from four other classifiers were omitted due to low accuracy. Lazy.IBK rooted in the Lazy family, in which the Lazy learners maintained the training data and does not do anything to data until the classification process started. Lazy learning is a learning technique in which generalization is delayed until a request is made to the system in which the system attempts to generalize the training data before obtaining queries outside the training data [36]. Similar to the k-nearest neighbor (KNN) algorithm, the key benefit obtained from using a lazy learning approach is that the target function will be approximated locally. Since the objective function is locally approximated for each machine query, lazy learning systems can solve several problems simultaneously and deal successfully with changes in the problem arena [33]. IBK is a classifier for the KNN that uses the same distance metric. It is an efficient algorithm for classification that can work with complex problems. Data can be well categorized with the use of the KNN classifier because there are thousands of attributes and the training range is broad in scale [37].

By utilizing Lazy.IBK classifier, the best data grouping was selected based on the highest percentage of correctly classified instances. As elaborated earlier, grouping 1 (non-grouping data), grouping 2 (by comparing 2 data), grouping 3, and grouping 4 were tested. Results in Table 3 showed that the percentage of correctly classified instances decreased from grouping 3 to grouping 4. Importantly, grouping 2 categorized the data with the highest correctly classified instances compared to others with 76.62%. It can also be observed that without grouping the data (grouping 1), the original value of the data showed the lowest percentage correctly classified instances with 68.98% only.

Based on grouping 2 and Lazy.IBK as the classifier output, the data were further analyzed to evaluate the accuracy of correctly classified data based on the thumb angle positions and conditions. Eight classes were developed to represent four thumb angle positions (zero-degree, thirty-degree, sixty-degree, and ninety-degree) in two different conditions (contract and relax). As the output, Table 4 demonstrates that in sum, 662 datasets with 76.62% were accurately (correctly) classified and 202 datasets with 23.38% were inaccurately (incorrectly) classified.

Table 3 - Summary of tested data grouping using Lazy IBK classifier

Group	Correctly Classified Instances (%)	Incorrectly Classified Instances (%)
1 Grouping 1	68.98	31.02
2 Grouping 2	76.62	23.38
3 Grouping 3	75.34	24.65
4 Grouping 4	74.65	25.35

Table 4 - Confusion matrix of grouping 2 using Lazy.IBK classifier

a	b	c	d	e	f	g	h	Class	Accuracy (%)	Precision (%)
84	16	6	1	0	1	0	0	a = zero-degree contract	77.78	80.77
15	88	0	4	1	0	0	0	b = zero-degree relax	81.48	79.28
3	0	76	13	10	2	3	1	c = thirty-degree contract	70.37	77.55
1	7	11	81	1	7	0	0	d = thirty-degree relax	75	76.42
1	0	4	2	78	14	8	1	e = sixty-degree contract	72.22	69.03
0	0	0	5	14	85	0	4	f = sixty-degree relax	78.7	73.91
0	0	1	0	9	1	88	9	g = ninety-degree contract	81.48	73.33
0	0	0	0	0	5	21	82	h = ninety-degree relax	75.92	84.53

	Accuracy (%)	Precision (%)
Contract	75.46	75.17
Relax	77.78	78.54
Average	76.62	76.85

From the table, it can be observed that most of the classes were successfully classified; with the highest accuracy, correctly classified data was class g (ninety-degree contract) and b (zero-degree relax) with 81.48% with 88 data correctly classified (and 20 data incorrectly classified). The highest precision was recorded by class h (ninety-degree relax) with a rate of 84.53%. correctly classified with 82 data correctly classified (and 15 data incorrectly classified). Meanwhile, the lowest accuracy was recorded by class c (thirty-degree contracts) with a percentage of 70.37% with 76 data correctly classified (and 32 data incorrectly classified) and the lowest precision was 69.03% for class e (sixty-degree contracts) with 78 data correctly classified and 35 data incorrectly classified.

Notably, the highest incorrectly classified data can be found for a class that contained the same thumb angle positions with opposite conditions (contract and relax). For example, class a (zero-degree contract) has 16 datasets which as incorrectly classified as class b (zero-degree relax). To distinctly differentiate the thumb's conditions (between contract and relax conditions), the data was then manipulated by inverting (or multiplying with -1) the relax data condition while the contract data condition has remained as it is. The final confusion matrix after inverting the relax data can be seen in Table 5.

As result, the percentage of correctly classified instances increased up to 89.58% (instead of 76.62% without inverting the relax condition) with 774 correctly classified datasets and 90 datasets (10.5%) incorrectly classified instances. These outputs demonstrated that the confusion in between different conditions (relax and contract conditions) for the same angle thumb position has been abolished. To illustrate, in class a (zero-degree contract), the accuracy data correctly classified instances have increased to 93.52% (instead of 77.78% from Table 4) with 101 datasets successfully classified. It means that there was no data for the zero-degree contract was incorrectly classified as class b (zero-degree relax).

Table 5 - Final confusion matrix of grouping 2 using Lazy.IBK classifier by inverting relax condition.

a	b	c	d	e	f	g	h	Class	Accuracy (%)	Precision (%)
101	0	7	0	0	0	0	0	a = zero-degree contract	93.52	96.19
0	103	0	5	0	0	0	0	b = zero-degree relax	95.37	93.64
3	0	92	0	9	0	4	0	c = thirty-degree contract	85.19	85.98
0	7	0	94	0	7	0	0	d = thirty-degree relax	87.04	88.68
1	0	5	0	92	0	10	0	e = sixty-degree contract	85.19	90.2
0	0	0	6	0	97	0	5	f = sixty-degree relax	89.81	87.39
0	0	3	0	10	0	95	0	g = ninety-degree contract	87.96	86.24
0	0	0	1	0	7	0	100	h = ninety-degree relax	92.59	95.24

	Accuracy (%)	Precision (%)
Contract	87.96	89.65
Relax	91.2	91.24
Average	89.58	90.45

By comparing all classes, results demonstrated that class b (zero-degree relax) showed the highest accuracy with 103 data were correctly classified, followed by class a (zero-degree contract) with 101 datasets correctly classified and class h (ninety-degree relax) with 100 datasets. Out of 108 data, all these three classes (a, b, h) demonstrated more than 100 classified data and have an accuracy of 95.37 % for zero-degree relax (class b) and 93.52 % for contraction state (class a) while ninety-degree relax condition showed 92.59% accuracy (class h). The lowest accuracy rate recorded was 85.19%, represented by thirty-degree angle contraction (class c) and sixty-degree angle muscle contraction (class e) with 92 datasets were correctly be classified. Overall, the final confusion matrix showed that Lazy.IBK with grouping 2 (with inverted relax condition) successfully classify the forearm HD-sEMG signals for the anterior compartment with high accuracy and high precision.

4. Conclusion

This study investigates the human forearm extrinsic muscle activity in order to characterize different thumb attitudes. HD-sEMG is the method used to capture the EMG signals at the extrinsic muscles during different thumb attitudes fixed at zero-degrees, thirty-degree, sixty-degrees, and ninety-degrees respectively. The analysis and classification have been successfully performed using Weka software and the results showed different levels of correctly classified instance percentages for different classifiers and groups. The highest correctly classified instances are 89.58% which was obtained using Lazy.IBK grouping 2. Future improvements to this study can be achieved by including additional HD-sEMG measurements collected from the posterior forearm muscles and also exploring other feature extraction methods.

Acknowledgement

The authors would like to acknowledge the support from the Ministry of Education Malaysia under Grant FRGS/1/2019/TK04/UIAM/02/5, participants in this study, and all the members of BioMechatronic Research Laboratory IIUM.

References

- [1] W. F. Xu, Y. F. Fang, G. Y. Zhang, Z. J. Ju, G. F. Li, and H. H. Liu, "Surface Emg Channel Selection for Thumb Motion Classification signal," *Proc. - Int. Conf. Mach. Learn. Cybern.*, vol. 2, pp. 662–666, 2018, doi: 10.1109/ICMLC.2018.8526988.
- [2] Alejandra Aranceta-Garza* and Bernard Arthur Conway, "Differentiating Variations in Thumb Position From Recordings of the Surface Electromyogram in Adults Performing Static Grips , a Proof of Concept Study," vol. 7, no. May, pp. 1–11, 2019, doi: 10.3389/fbioe.2019.00123.
- [3] N. Ha, G. P. Withanachchi, and Y. Yihun, "Performance of Forearm FMG for Estimating Hand Gestures and Prosthetic Hand Control," vol. 16, pp. 88–98, 2019.
- [4] P. Maduri and H. Akhondi, "Upper Limb Amputation.," StatPearls., Treasure Island, Treasure Island (FL): StatPearls Publishing, Treasure Island (FL), 2020.
- [5] Y. Li, K. Kulbacka-Ortiz, K. Caine-Winterberger, and R. Brånemark, "Thumb Amputations Treated With

- Osseointegrated Percutaneous Prostheses With Up to 25 Years of Follow-up.,” *J. Am. Acad. Orthop. Surg. Glob. Res. Rev.*, vol. 3, no. 1, p. e097, Jan. 2019, doi: 10.5435/JAAOSGlobal-D-18-00097.
- [6] J. A. Birdwell, L. J. Hargrove, R. F. Weir, and T. A. Kuiken, “Extrinsic finger and thumb muscles command a virtual hand to allow individual finger and grasp control,” *IEEE Trans. Biomed. Eng.*, vol. 62, no. 1, pp. 218–226, 2015, doi: 10.1109/TBME.2014.2344854.
- [7] C. J. de Luca, “Physiology and Mathematics of Myoelectric Signals,” *IEEE Trans. Biomed. Eng.*, vol. BME-26, no. 6, pp. 313–325, 1979, doi: 10.1109/TBME.1979.326534.
- [8] R. N. Khushaba, A. H. Al-Timemy, A. Al-Ani, and A. Al-Jumaily, “A Framework of Temporal-Spatial Descriptors-Based Feature Extraction for Improved Myoelectric Pattern Recognition,” *IEEE Trans. Neural Syst. Rehabil. Eng.*, vol. 25, no. 10, pp. 1821–1831, 2017, doi: 10.1109/TNSRE.2017.2687520.
- [9] U. Wijk and I. Carlsson, “Forearm amputees’ views of prosthesis use and sensory feedback,” *J. Hand Ther.*, vol. 28, no. 3, pp. 269–278, 2015, doi: 10.1016/j.jht.2015.01.013.
- [10] E. Mastinu *et al.*, “Grip control and motor coordination with implanted and surface electrodes while grasping with an osseointegrated prosthetic hand,” vol. 2, pp. 1–10, 2019.
- [11] M. U. Atique and K. S. Rabbani, “A Cost-Effective Myoelectric Prosthetic Hand,” no. October, 2018, doi: 10.1097/JPO.000000000000211.
- [12] R. F. ff W. Christian Cipriani, Jacob L. Segil, J. Alex Birdwell, “Dexterous Control of a Prosthetic Hand Using Fine-Wire Intramuscular Electrodes in Targeted Extrinsic Muscles,” *HHS Public Access*, vol. 22, no. 4, pp. 828–836, 2015, doi: 10.1109/TNSRE.2014.2301234.Dexterous.
- [13] M. A. C. Garcia and T. M. M. Vieira, “Surface electromyography: Why, when and how to use it,” *Med. del Deport.*, vol. 4, no. 1, pp. 17–28, 2011.
- [14] D. F. Stegeman, B. U. Kleine, and B. G. Lapatki, “High-density Surface EMG : Techniques and Applications at a Motor Unit Level,” *Biocybern. Biomed. Eng.*, vol. 32, no. 3, pp. 3–27, 2012, doi: 10.1016/S0208-5216(12)70039-6.
- [15] A. Boschmann and M. Platzner, “Towards Robust HD EMG Pattern Recognition : Reducing Electrode Displacement Effect using Structural Similarity,” pp. 4547–4550, 2014.
- [16] M. Jordanic, M. Rojas-martínez, M. A. Mañanas, and J. F. Alonso, “Spatial distribution of HD-EMG improves identification of task and force in patients with incomplete spinal cord injury,” *J. Neuroeng. Rehabil.*, pp. 1–11, 2016, doi: 10.1186/s12984-016-0151-8.
- [17] A. R. Siddiqi and S. N. Sidek, “Estimation of continuous thumb angle and force using electromyogram classification,” *Int. J. Adv. Robot. Syst.*, vol. 13, no. 5, pp. 1–12, 2016, doi: 10.1177/1729881416658179.
- [18] M. Hakonen, H. Piitulainen, and A. Visala, “Biomedical Signal Processing and Control Current state of digital signal processing in myoelectric interfaces and related applications,” *Biomed. Signal Process. Control*, vol. 18, pp. 334–359, 2015, doi: 10.1016/j.bspc.2015.02.009.
- [19] S. S. G. Dupan, D. F. Stegeman, and H. Maas, “Distinct neural control of intrinsic and extrinsic muscles of the hand during single finger pressing,” *Hum. Mov. Sci.*, vol. 59, no. April, pp. 223–233, 2018, doi: 10.1016/j.humov.2018.04.012.
- [20] A. Phinyomark, P. Phukpattaranont, and C. Limsakul, “Expert Systems with Applications Feature reduction and selection for EMG signal classification,” *Expert Syst. Appl.*, vol. 39, no. 8, pp. 7420–7431, 2012, doi: 10.1016/j.eswa.2012.01.102.
- [21] S. Electromyography, S. Processing, and C. Techniques, “Surface Electromyography Signal Processing and Classification Techniques,” pp. 12431–12466, 2013, doi: 10.3390/s130912431.
- [22] N. J. Cronin, S. Kumpulainen, T. Joutjärvi, T. Finni, and H. Piitulainen, “Spatial variability of muscle activity during human walking: The effects of different EMG normalization approaches,” *Neuroscience*, vol. 300, pp. 19–28, 2015, doi: 10.1016/j.neuroscience.2015.05.003.
- [23] S. F. S. Syeda Farha Shazmeen, “Performance Evaluation of Different Data Mining Classification Algorithm and Predictive Analysis,” *IOSR J. Comput. Eng.*, vol. 10, no. 6, pp. 1–6, 2013, doi: 10.9790/0661-1060106.
- [24] A. S. Ghazali, S. N. Sidek, and S. Wok, “Affective state classification using Bayesian classifier,” *Proc. - Int. Conf. Intell. Syst. Model. Simulation, ISMS*, vol. 2015-Septe, pp. 154–158, 2015, doi: 10.1109/ISMS.2014.32.
- [25] Y. L. Ng, X. Jiang, Y. Zhang, S. B. Shin, and R. Ning, “Automated Activity Recognition with Gait Positions Using Machine Learning Algorithms,” *Eng. Technol. Appl. Sci. Res.*, vol. 9, no. 4, pp. 4554–4560, 2019, doi: 10.48084/etasr.2952.
- [26] A. Nait-ali, W. Biometric, and S. Meets, “Towards High Density sEMG (HD-sEMG) Acquisition Approach for Biometrics Applications,” in *Hidden Biometrics: When Biometric Security Meets Biomedical Engineering*, Springer Nature Singapore Pte Ltd, 2019, pp. 101–112.
- [27] X. Bao, Y. Zhou, Y. Wang, J. Zhang, X. Lu, and Z. Wang, “Electrode placement on the forearm for selective stimulation of finger extension / flexion,” no. 61534003, pp. 1–22, 2018.
- [28] P. Taylor, A. Samani, A. Holtermann, K. Søgaard, and A. Holtermann, “Following ergonomics guidelines decreases physical and cardiovascular workload during cleaning tasks,” no. June 2013, pp. 37–41, 2011.
- [29] D. Thompson, I. A. N. G. Mackenzie, and H. Leuthold, “Emotional responses to irony and emoticons in written

- language : Evidence from EDA and facial EMG,” vol. 53, pp. 1054–1062, 2016, doi: 10.1111/psyp.12642.
- [30] P. Ghaderi and H. R. Marateb, “Muscle activity map reconstruction from high density surface EMG signals with missing channels using image inpainting and surface reconstruction methods,” *IEEE Trans. Biomed. Eng.*, vol. 64, no. 7, pp. 1513–1523, 2017, doi: 10.1109/TBME.2016.2603463.
- [31] J. Bashford *et al.*, “Clinical Neurophysiology Preprocessing surface EMG data removes voluntary muscle activity and enhances SPiQE fasciculation analysis,” *Clin. Neurophysiol.*, vol. 131, no. 1, pp. 265–273, 2020, doi: 10.1016/j.clinph.2019.09.015.
- [32] A. Hegyi, A. Péter, T. Finni, and N. J. Cronin, “Region-dependent hamstrings activity in Nordic hamstring exercise and stiff-leg deadlift defined with high-density electromyography,” *Scand. J. Med. Sci. Sport.*, vol. 28, no. 3, pp. 992–1000, 2018, doi: 10.1111/sms.13016.
- [33] G. Krishna, B. Kumar, N. Orsu, and S. B., “Performance Analysis and Evaluation of Different Data Mining Algorithms used for Cancer Classification,” *Int. J. Adv. Res. Artif. Intell.*, vol. 2, no. 5, pp. 49–55, 2013, doi: 10.14569/ijarai.2013.020508.
- [34] E. Frank, M. Hall, G. Holmes, R. Kirkby, and I. H. Witten, “Data Mining and Knowledge Discovery Handbook,” *Data Min. Knowl. Discov. Handb.*, no. July, pp. 0–10, 2010, doi: 10.1007/978-0-387-09823-4.
- [35] I. H. Witten, E. Frank, and M. A. Hell, “Data Mining : Practical Machine Learning Tools and Technique , Third Edition,” vol. 36, no. 5, pp. 51–52, 2011, doi: 10.1145/2020976.2021004.
- [36] M. S. Vijayarani, M. M. Muthulakshmi, and A. Professor, “Comparative Analysis of Bayes and Lazy Classification Algorithms,” *Int. J. Adv. Res. Comput. Commun. Eng.*, vol. 2, no. 8, 2013, [Online]. Available: www.ijarccce.com.
- [37] Y. Liu and G. S. Chen, “KNN algorithm improving based on Cloud Model,” *Proc. - 2nd IEEE Int. Conf. Adv. Comput. Control. ICACC 2010*, vol. 2, pp. 63–66, 2010, doi: 10.1109/ICACC.2010.5487185.